

scJoint: transfer learning for data integration of single-cell RNA-seq and ATAC-seq

Yingxin Lin^{1,2§}, Tung-Yu Wu^{3§}, Sheng Wan⁴, Jean Y.H. Yang^{1,2}, Y. X. Rachel Wang^{1*}, and Wing H. Wong^{3,5,6*}

¹School of Mathematics and Statistics, The University of Sydney, NSW, Australia.

²Charles Perkins Centre, The University of Sydney, NSW, Australia.

³Department of statistics, Stanford University, CA, USA.

⁴Institute of Electronics, National Chiao Tung University, Hsinchu, Taiwan.

⁵Department of Biomedical Data Science, Stanford University, CA, USA.

⁶Bio-X Program, Stanford University, CA, USA.

[§]Equal contribution.

*To whom correspondence should be addressed. Email: Y. X. Rachel Wang, rachel.wang@sydney.edu.au; Wing H. Wong, whwong@stanford.edu.

Abstract

Single-cell multi-omics data continues to grow at an unprecedented pace, and while integrating different modalities holds the promise for better characterisation of cell identities, it remains a significant computational challenge. In particular, extreme sparsity is a hallmark in many modalities such as scATAC-seq data and often limits their power in cell type identification. Here we present scJoint, a transfer learning method to integrate heterogeneous collections of scRNA-seq and scATAC-seq data. scJoint uses a neural network to simultaneously train labelled and unlabelled data and embed cells from both modalities in a common lower dimensional space, enabling label transfer and joint visualisation in an integrative framework. We demonstrate scJoint consistently provides meaningful joint visualisations and achieves significantly higher label transfer accuracy than existing methods using a complex cell atlas data and a biologically varying multi-modal data. This suggests scJoint is effective in overcoming the heterogeneity in different modalities towards a more comprehensive understanding of cellular phenotypes.

Introduction

Advances in single-cell technologies have enabled comprehensive studies of cell heterogeneity, developmental dynamics, and cell communications across diverse biological systems at an unprecedented resolution. There are a variety of protocols profiling the transcriptomics,

as exemplified by single-cell RNA-seq (scRNA-seq). In addition, a number of technologies have been developed for other molecular measurements in individual cells towards building a more holistic view of cell functions, including chromatin accessibility, protein abundance, and methylation (30).

In particular, single-cell ATAC-seq (scATAC-seq) is an epigenomic profiling technique for measuring chromatin accessibility to discover cell type specific regulatory mechanisms (6; 15). scATAC-seq offers a complementary layer of information to scRNA-seq, and together they provide a more comprehensive molecular profile of individual cells and their identities. However, it has been noted that the extreme sparsity of scATAC-seq data often limits its power in cell type identification (25). In contrast, large amounts of well-annotated scRNA-seq datasets have been curated as cell atlases (27; 26), motivating us to transfer cell type information from scRNA-seq to scATAC-seq for better classification of cell types in an integrative analysis framework.

A number of methods exist to denoise, batch correct, and perform integration of single-omics data across multiple experiments for both transcriptomic data (19; 32; 17; 16; 33; 3) and scATAC-seq data (36). However, direct applications of these methods to multi-omics data integration are computationally challenging and often suboptimal, since different modalities have vastly different dimensions and sparsity levels. Recently, a growing number of methods have been proposed to address the need for integrative analysis across different modalities. When the data consist of simultaneous multi-modal measurements within the same cell (8; 7), methods like scAI (13) and MOFA+ (4) have been developed for factor analysis and joint clustering. However, these paired measurements are technically more challenging and costly to perform. More commonly, different modalities are derived from different cells taken from the same or similar populations. In this setting, most existing methods are broadly based on manifold alignment (34; 2; 18) to match the distributions of different modalities globally in a latent space, matrix factorisation (Liger (35), coupledNMF (10)), or using correlations to identify nearby cells across modalities (Conos (5), Seurat (29)). While these methods have demonstrated promising results in integrating multiple modalities measured in cells from the same tissue, requiring distributions to match globally in manifold alignment may be too restrictive for more complex data compositions as typically seen in cell atlases, where measurements for different modalities are derived from different tissues and cell types. Furthermore, matrix factorisation and correlation-based methods often perform a separate feature selection step prior to integration for dimension reduction, and the method's performance can be sensitive to which genes are selected.

Here, we present an end-to-end transfer learning method, scJoint, that effectively integrates scRNA-seq and scATAC-seq data using a neural network approach. It is well established that in addition to having high prediction power, the hidden units of neural networks are able to learn implicit representations from the underlying data distribution (37). Hence, by leveraging information from annotated scRNA-seq datasets, we use the same encoder to simultaneously train the two modalities so that 1) implicit features reflecting the annotations can be learnt by a hidden layer in an embedding space, and 2) unlabelled data from the ATAC domain can be aligned to similar points in the same embedding space. In contrast to methods that need a preliminary dimension reduction step, scJoint contains **a novel loss function** to explicitly incorporate dimension reduction as part of the feature engineering process in trans-

fer learning, allowing the low dimensional features to be updated throughout training and removing the need for selecting highly variable genes. This integrative framework enables scJoint to transfer cell type labels from scRNA-seq to scATAC-seq data and construct a joint embedding for the two modalities. By applying scJoint to integrate two mouse cell atlases (scRNA-seq (27) and scATAC-seq (9)) and a multi-modal data with paired protein measurements, we demonstrate our method achieves considerably higher label transfer accuracy and integration quality over existing methods.

Results

scJoint for co-training labelled and unlabelled data

The core of scJoint is a semi-supervised approach to co-train labelled data (scRNA-seq) and unlabelled data (scATAC-seq), where we address the main challenge of aligning these two distinct data modalities via a common lower dimensional space. scJoint consists of three main steps (Figure 1a). Step 1 performs joint dimension reduction and modality alignment in a common embedding space through a novel neural network based dimension reduction (NNDR) loss and a cosine similarity loss respectively. The NNDR loss extracts orthogonal features with maximal variability in a vein similar to PCA, while the cosine similarity loss encourages the neural network to find projections into the embedding space so that majority parts of the two modalities can be aligned. The embedding of scRNA-seq is further guided by a cell type classification loss, forming the semi-supervised part. In Step 2, treating each cell in scATAC-seq data as a query, we identify the k-nearest neighbours (KNN) among scRNA-seq cells by measuring their distances in the common embedding space, and transfer the cell type labels from scRNA-seq to scATAC-seq via majority vote. In Step 3, we further improve the mixing between the two modalities by utilising the transferred labels in a metric learning loss. Joint visualisation of the datasets is obtained from the final embedding layer using standard tools including tSNE (20) and UMAP (22). scJoint requires simple data preprocessing with the input dimension equal to the number of genes in the given datasets after appropriate filtering. Chromatin accessibility in scATAC-seq data is first converted to gene activity scores (24; 31) allowing for the use of a single encoder with weight sharing for both RNA and ATAC.

We next compared scJoint with methods recently developed and applied to the integration of scRNA-seq and scATAC-seq, including Seurat v3 (29), Conos (5) for label transfer accuracy, and additionally Liger (35) (as a representative matrix factorisation method) for evaluating the joint embedding of the two modalities.

scJoint shows accurate and robust performance on large atlas data.

We demonstrate the performance of scJoint in a complex scenario, where the heterogeneity of cell types and tissues in atlas data poses significant challenges to data integration. We applied our method to integrate two mouse cell atlases: the Tabula Muris atlas (27) for scRNA-seq data and the atlas in (9) for scATAC-seq data, containing 73 cell types (96,404 cells from 20 organs, two protocols) and 29 cell types (81,173 cells from 13 tissues) respectively (the latter including a group annotated as ‘unknown’), of which 19 cell types are common. We focus our initial evaluation on the subset of the atlas data containing 101,692 cells from the

19 overlapping cell types only. Here, we transferred cell type labels from scRNA-seq to scATAC-seq and compared the results with the original labels in (9) for accuracy; these original labels were also used to evaluate the quality of joint visualisations. An inspection of the tSNE plots shows our method effectively mixes the three protocols (FACS, droplet, ATAC) while providing a better grouping of the cells in terms of previously defined cell types than the other methods (Figure 2a, Supplementary Figure S1). This observation is confirmed by the quantitative evaluation metrics, with scJoint showing significantly higher cell type silhouette coefficients than all the other methods and similar modality silhouette coefficients as Seurat and Liger. Overall, scJoint has the highest median F1-score of silhouette coefficients, achieving a better trade-off between removing the technological variations in modalities and maintaining the cell type signals (Figure 2b, Supplementary Figure S2). In terms of label transfer accuracy, scJoint assigned 84% of the cells to the correct type, 14% and 13% higher than Seurat and Conos (Figure 2d, Supplementary Figure S3).

To assess the robustness of the label transfer results, we performed a stability analysis on this subset of atlas data by subsampling 80%, 50%, 20% of the cells from scRNA-seq as the training data. Even when only 20% of the cells were used for training, scJoint maintained a high accuracy and small variance (Figure 2c), suggesting that scJoint is potentially applicable to situations where only a subset of the scRNA-seq data is annotated.

Label transfer using highly heterogeneous atlas data refines cell type annotations in scATAC-seq.

We next performed the more challenging task of integrating the full atlas data. Since the scRNA-seq atlas contains more cell types than the scATAC-seq atlas, we use this application to illustrate how transferred labels can refine and provide new annotations to ATAC cells. To compare with the original labels, tSNE plots were constructed in the same way as (9), using singular value decomposition of the term frequency-inverse document frequency (TF-IDF) transformation of scATAC-seq peak matrix (Figure 3a). We observe that scJoint labels cells close together in this ATAC visualisation space in a more consistent way than the other methods. Qualitatively this is supported by scJoint's higher overall accuracy rate (77% compared with 60% for Seurat and 55% for Conos).

Examining the transferred labels further, we find scJoint labels a group of cells (originally labelled as 'unknown' or 'endothelials') as 'stromal cells' (4352 cells) and 'fibroblasts' (1602 cells), which are two cell types not present in the original ATAC labels. These cells show high gene activity scores for *Col1a1*, *Col1a2*, *Dcn* and *Ccdc80*, all of which are markers with high expression levels in stromal cells and fibroblasts but low expression levels in endothelial cells from the scRNA-seq data (Figure 3b). Hence, the new annotations are more consistent with the marker expression levels.

More interestingly, we note scJoint allows us to annotate 5931 cells labelled as 'unknown' in (9) with probability score greater than 0.80. These cells are clearly clustered into groups in the tSNE visualisation of scJoint's embedding space (Figure 3c), with the main groups being endothelial cells, stromal cells, neurons and B cells. Using cell type markers identified from the scRNA-seq data, the aggregated gene activity scores of these ATAC cells show clear differential expression patterns (Figure 3d).

scJoint enables accurate integration of single-cell multi-modal data across biological conditions.

We demonstrate scJoint is capable of incorporating additional modality information to RNA-seq and ATAC-seq and applicable to experiments with different underlying biological conditions. We consider multi-modal measurements profiling gene expression levels or chromatin accessibility simultaneously with surface protein levels, which can be obtained via CITE-seq (28) and ASAP-seq (23). We analysed CITE-seq and ASAP-seq data from a T cell stimulation experiment in (23), which sequenced cells with these two technologies in parallel. A total of 18,088 cells were studied under two conditions: one with stimulation of anti-CD3/CD28 in the presence of IL-2 for 16 hours and the other without stimulation as control. We first clustered and annotated these cells using CiteFuse (14). Compared to the cell type labels in the original study, we were able to identify cellular subtypes with CiteFuse, further annotating five subgroups in T cells. Next, we performed integration analysis of CITE-seq and ASAP-seq by concatenating gene expression or gene activity vectors with protein measurements. The analysis was performed in two scenarios: within the stimulated and control condition separately and across the two conditions.

In both scenarios, scJoint generated a better joint visualisation of the two technologies (Figure 4a, Supplementary Figures S4, S5). In particular, in the case where stimulated and control cells are combined, subtypes of T cells (e.g. naive CD8+, effector CD8+, naive CD4+, and effector CD4+) are clearly separated while cells from the two technologies are well mixed (Figure 4a, 4b). The median cell type silhouette coefficient of scJoint is 0.51, outperforming the other three methods by a large margin (Seurat 0.11, Conos 0.13, and Liger -0.06). With the highest silhouette coefficient F1 scores (median F1 score: 0.59) representing a 16% - 28% improvement over the other methods, scJoint demonstrates the best balance between removing technical variations and preserving biological signals (Figure 4c).

Moreover, scJoint achieves higher accuracy in label transfer under all scenarios (88% in control, 84% in stimulation, and 87% in the combined case), compared with Seurat (80% in control, 79% in stimulation, and 75% combined) and Conos (53% in control, 67% in stimulation, and 56% in combined) (Figure 4d and Supplementary Figure S7). In addition, the transferred labels of scJoint from the two scenarios (control / stimulation alone, and combined) are highly consistent, with 95% of cells having the same annotation, substantially greater than Seurat (84%) and Conos (59%) (Supplementary Figure S8).

Integration of multi-modal data with scJoint captures additional biological signals in cell types and conditions

In the combined analysis of stimulation and control, we find that the joint embedding generated by scJoint contains additional information that allows for the identification of a cellular subtype. In the CiteFuse annotation of ASAP-seq data, we labelled one cluster of 142 cells with ambiguous marker expression as ‘unknown’. Interestingly, in the joint visualisation of scJoint, while these ‘unknown’ cells are labelled as ‘natural killer cells (NK)’ by label transfer, they are still clearly separated from the majority of NK cells and form a small cluster together with cells from CITE-seq. We then examined the gene and protein expression levels of NK cell and T cell markers in this subgroup. We find these cells have high expression of

CD3 and GNLY at gene level as well as CD3, CD56, CD57, and CD244 at protein level, but low expression of CD8A and CD4. This suggests these cells may be natural killer T cells, a minority of immune cells in PBMC sample (Figure 4e, Supplementary Figure S9b) (12). By contrast, although these cells lack CD8 expression, the other methods are unable to distinguish them from effector CD8+ T cells in their visualisations (Figure 4e, Supplementary Figure S10).

Lastly, by appropriately aligning the two technologies in the embedding space, scJoint is able to reveal the biological difference between stimulation and control within the same cell type. In the joint visualisation of scJoint, three subtypes of T cells (naive CD4+, naive CD8+, effector CD4+) are less well mixed between the two conditions than the other cell types, consistent with the stimulation experiment aiming to activate T cells. In particular, the naive CD4+ T cells show the most notable separation between the two conditions (Figure 4a). We then performed differential expression analysis of the scRNA-seq part of CITE-seq within each cell type across the two conditions using MAST (11). We find that the naive CD4+ T cells have the largest number of unique differentially expressed genes ($FDR < 0.01$) (Supplementary Figure S11a). Similarly, differential proteins analysis of both CITE-seq and ATAC-seq using wilcoxon rank sum test on the log-transformed protein abundances also suggests that naive CD4+ T cells have the most unique differential proteins compared with other cell types ($FDR < 0.01$) (Supplementary Figure S11b-c).

scJoint shows versatile performance on paired measurements of scRNA-seq and scATAC-seq.

Although scJoint is designed for integrating unpaired data, it is still directly applicable to paired data. Such an application also enables us to compare its performance with methods that incorporate pairing information and use the pairing information to validate the label transfer results. We consider the integration of adult mouse cerebral cortex data generated by SNARE-seq (8), a technology that can profile gene expression and chromatin accessibility in the same cell. In addition to Seurat and Liger, we compared scJoint with two other methods designed specifically for paired data, scAI (13) and MOFA+ (4). In our assessment, all the unpaired methods (scJoint, Seurat, Liger) treat the RNA and ATAC parts of SNARE-seq as two separate datasets, while the paired methods take the pairing information into account. We find that scJoint is able to provide clear groupings of cells according to cellular subtypes (Figure 5a) and achieves comparable or better cell type silhouette coefficients (Figure 5b) than the paired methods. This suggests that scJoint is versatile enough to be applied to paired data, which are becoming increasingly popular.

Comparing the performance among the unpaired methods, scJoint has the highest medians in cell type silhouette coefficients and F1-scores (Figure 5b, S13). For label transfer, scJoint achieves an accuracy rate of 70.9%, retaining better performance than the other two methods (70.1% for Seurat and 49.5% for Conos). Looking closer at the performance in each cell type, scJoint performs the best in 10 out of 22 cell types in terms of F1 scores for classification (Supplementary Figure S14). Together, these results suggest that scJoint performs the best among the unpaired methods and on par with the paired methods, despite treating paired data as separate.

Discussion

scJoint approaches the integration of scRNA-seq and scATAC-seq as a domain adaptation problem in transfer learning, using the same neural network to co-train labelled data from the source domain (RNA) and unlabelled data from the target domain (ATAC) following a different distribution. scRNA-seq data serve as a natural source domain for transferring information to other modalities due to rapidly growing collections of annotated public data and RNA-focused computational tools that can output accurate classifications (1). Using mouse cell atlases and multi-modal data with protein measurements, we demonstrate scJoint achieves significantly higher label transfer accuracy and provides better joint visualisations than other methods even when 1) the data is highly complex and heterogeneous and 2) meaningful biological conditions are mixed with technical variations. We have shown that integrative analysis of single-cell multi-omics data by scJoint facilitates re-annotation of cell types in scATAC-seq and discovery of new subtypes not present in training data.

scJoint provides a concise training framework with one main tuning parameter in the construction of cosine similarity loss. As shown in Supplementary Figure S16a, our results are quite stable with respect to the choice of this parameter. Similar to other methods based on neural networks, the number of hidden nodes in the architecture and other optimisation details can be considered tunable as well, although they do not appear to affect our results (Supplementary Figure S16a-b).

The superior performance and robustness of scJoint illustrate its utility as a tool to automatically label cells from other modalities given an annotated scRNA-seq database. By embedding all cells in a common lower dimensional space, scJoint assigns a probability score to a cell type prediction by combining the softmax probabilities of its nearest neighbours. As we vary the level of cutoff, the accuracy of scJoint still consistently outperforms the other methods (Supplementary Figure S15). The robustness of scJoint was demonstrated through subsampling experiments, where the stability of our results implies the method can be applied to partially labelled databases. Despite being a semi-supervised method guided by labelled data, the dimension reduction component in our design lends it sufficient flexibility to preserve implicit data signals, including biological variations induced by experimental conditions and additional cellular subtypes. One can conceivably extend scJoint to an unsupervised setting, replacing the softmax prediction layer with a decoder minimising reconstruction loss.

Although designed for unpaired data, scJoint is still directly applicable to paired data and generates joint visualisations with cells coherently grouped by cell types. In the current training scheme, the pairing information between RNA and ATAC is only used to validate the label transfer results. We expect that adapting scJoint to take paired vectors during training would enhance its performance on this type of data, and this would be especially useful in the unsupervised setting mentioned above.

We have focused on scATAC-seq as an example of epigenomic data, but in principle scJoint extends to other modalities such as methylation data, provided the input can be summarised as gene-level scores. While the gene-level summaries are amenable to generalisation and widely adopted by unpaired integration methods, this step itself is also a limitation as improper aggregation can incur information loss. Extending scJoint to directly handle epige-

nomic data at locus level will require designing a separate encoder that is suitable for the high dimensionality and remains easy to train, and we will pursue this for future work.

In summary, we have developed scJoint as a generalisable transfer learning method for performing integrative analysis of single-cell multi-omics data. scJoint was shown to effectively integrate multiple types of measurements from both unpaired or paired profiling, outperforming other methods in label transfer accuracy and providing joint visualisations that remove technical variations while preserving meaningful biological signals. scJoint's ability to integrate multi-omics data by capturing various aspects of cell characteristics unique to different data modalities will facilitate a more comprehensive view of cell functions and cell communications.

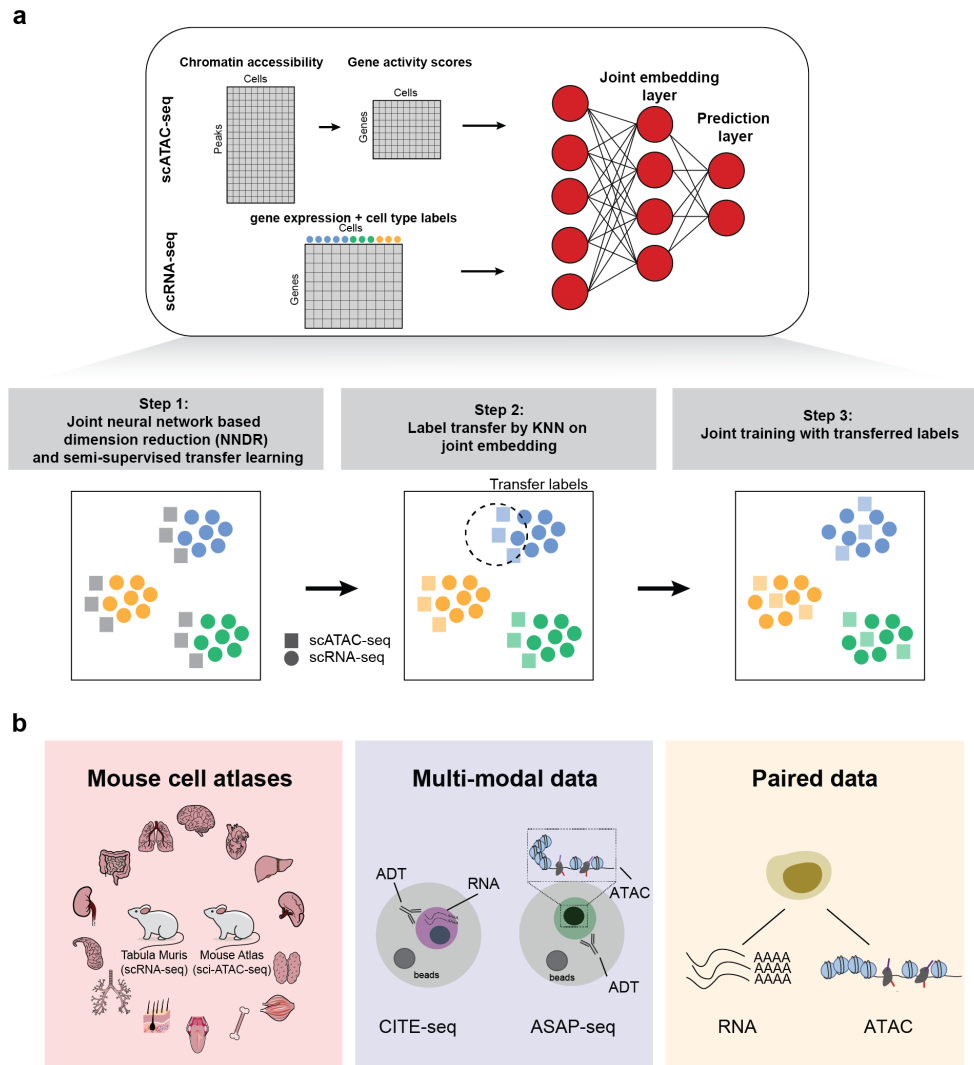


Figure 1: (a) Overview of scJoint. The input of scJoint consists of one (or multiple) gene activity score matrix, calculated from the accessibility peak matrix of scATAC-seq, and one (or multiple) gene expression matrix including cell type labels from scRNA-seq experiments. The method has three main steps: (1) Joint NNDR and semi-supervised transfer learning; (2) Cell type label transfer by k-nearest neighbour in joint embedding space; (3) Joint training with transferred labels. (b) Three data collections used in this study: (1) Mouse cell atlases; (2) Multi-modal data from PBMC; (3) Paired data from adult mouse cerebral cortex data generated by SNARE-seq.

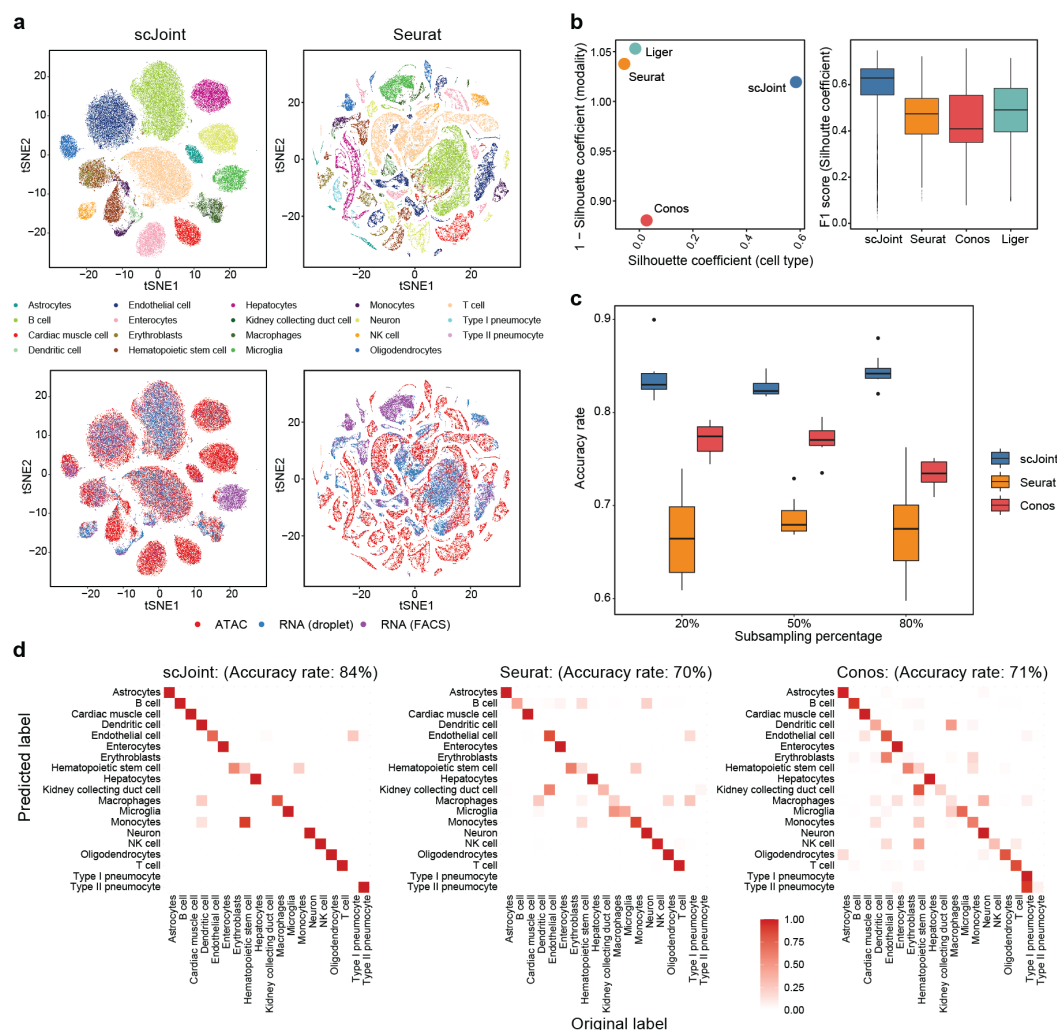


Figure 2: Analysis of mouse cell atlas subset data containing 19 overlapping cell types from RNA and ATAC. (a) tSNE visualisation of scJoint (left column) and Seurat (right column), coloured by cell types defined in (9) (first row) and three protocols (second row). (b) Scatter plot of mean silhouette coefficients for scJoint, Liger, Seurat, and Conos (left panel), where the x-axis shows the mean cell type silhouette coefficients and the y-axis shows '1 - mean modality silhouette coefficients'; ideal outcomes would lie in the top right corner. Boxplots of F1 scores of silhouette coefficients for scJoint, Liger, Seurat, and Conos (right panel). (c) Accuracy rates of scJoint, Seurat and Conos using 20%, 50% and 80% of cells from scRNA-seq data as training data. 10 random subsamplings were performed for each setting to generate the variance. (d) Predicted cell types and their fractions of agreement with the original cell types given in (9) for scJoint (left panel), Seurat (middle panel) and Conos (right panel). Clearer diagonal structure indicates better agreement.

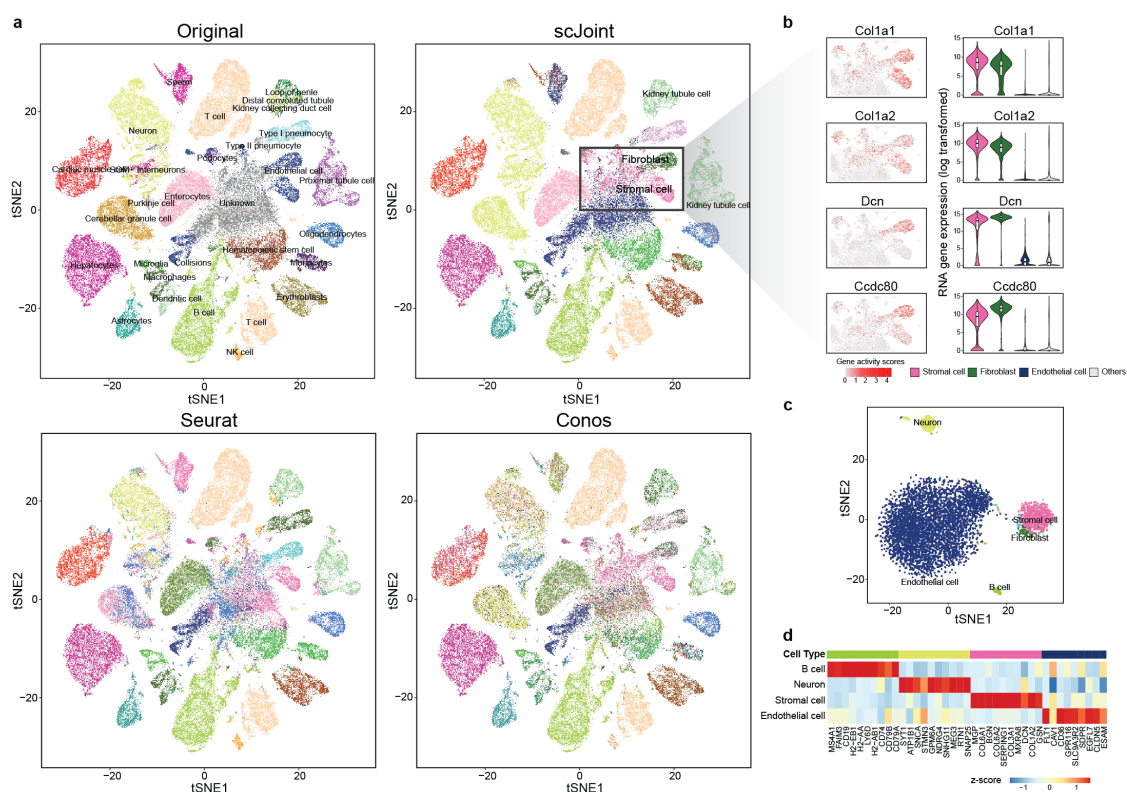


Figure 3: Analysis of mouse cell atlas full data. (a) A 2×2 panel of tSNE plots generated from top 100 dimensions of singular value decomposition of the TF-IDF transformed ATAC-seq data, coloured by the original labels (top left), scJoint transferred labels (top right), Seurat transferred labels (bottom left), and Conos transferred labels (bottom right). (b) Marker expressions in stromal cells and fibroblasts: Col1a1, Col1a2, Dcn and Ccdc80. The left column shows the gene activity scores of the markers in ATAC-seq data (4352 stromal cells, and 1602 fibroblasts). The right column shows the log-transformed gene expression of the markers in stromal cells, fibroblasts, endothelial cells versus others; all cells here are taken from the FACS scRNA-seq data. (c) tSNE plot of cells originally labelled as “unknown” and annotated by scJoint with probability scores greater than 0.80, coloured by predicted cell types (5931 cells). (d) Heatmap of z-scores of average gene activity scores, calculated from cells aggregated by predicted cell types in ATAC. The rows indicate the top four predicted cell types by size. The columns indicate the top differential expressed genes of the corresponding cell type in RNA.

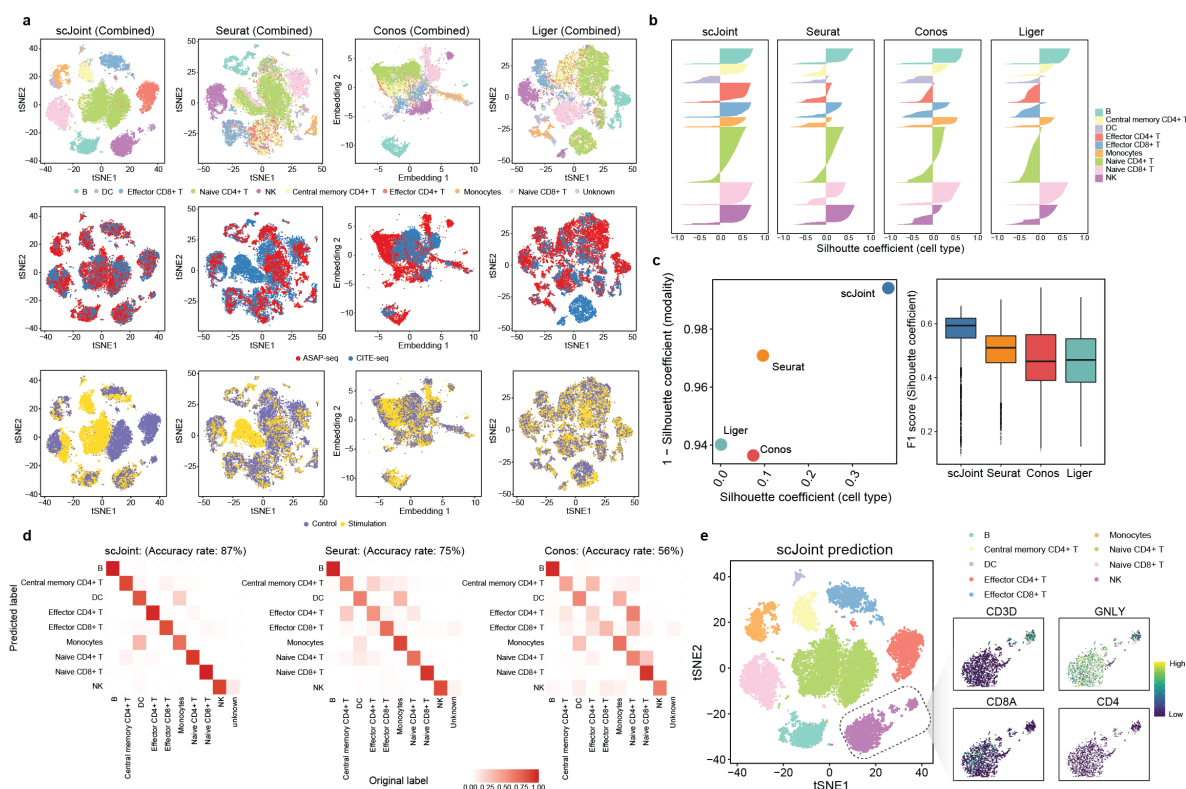


Figure 4: Integration of multi-modal PBMC data across biological conditions. (a) tSNE visualisation of scJoint (first column), Seurat (second column), Conos (third column) and Liger (fourth column) of PBMC data generated from CITE-seq and ASAP-seq, coloured by cell type obtained from CiteFuse and manual annotations (first row), technology (second row), and biological condition (third row). (b) Barplots of cell type silhouette coefficients for scJoint, Seurat, Conos and Liger for all cells, coloured by cell type. Larger values on the x-axis indicate better grouping. (c) Scatter plot of mean silhouette coefficients for scJoint, Seurat, Conos and Liger (left), where the x-axis denotes the mean cell type silhouette coefficients, and the y-axis denotes 1 - mean modality silhouette coefficients; ideal outcomes would lie in the top right corner. Boxplots of F1 scores of silhouette coefficients for scJoint, Liger, Seurat, and Conos (right). (d) Heatmaps comparing the original labels and the transferred labels of scJoint, Seurat and Conos. Clearer diagonal structure indicates better agreement. (e) tSNE visualisation of scJoint coloured by the predicted cell types with gene expression levels of CD3D, NKG7, CD8A and CD4 in natural killer cells.

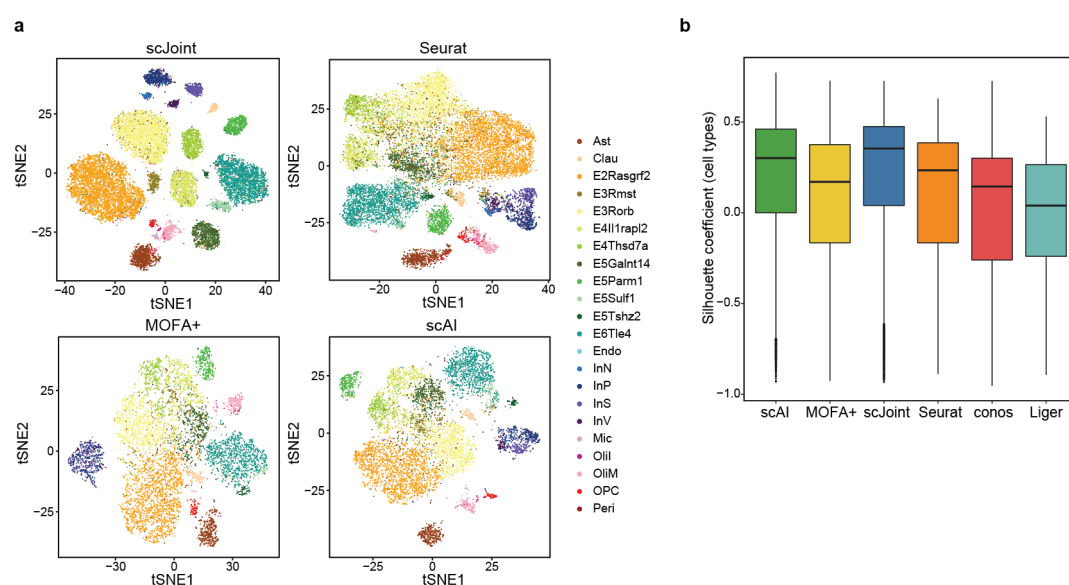


Figure 5: Analysis of paired gene expression and chromatin accessibility data from SNARE-seq. (a) tSNE visualisation of SNARE-seq data for scJoint, Seurat, MOFA+ and scAI, coloured by cell types given in (8). All unpaired methods treat the RNA and ATAC parts of SNARE-seq as two separate data. (b) Boxplots of cell type silhouette coefficients for scJoint, Seurat, Conos and Liger, coloured by methods.

Methods

Architecture and training of scJoint

The neural network in scJoint consists of one input layer and two fully connected layers. The input layer has dimension equal to the number of genes common to the expression matrix of scRNA-seq and the gene activity matrix of scATAC-seq, after simple filtering (see Data preprocessing). Now that the two modalities have matching input features, we co-train them using the same encoder which is equivalent to weight sharing. The first fully connected layer has 64 neurons with linear activation and serves as the joint low dimensional embedding space that captures aligned features from all cells. Visualisations of clustering structure can be obtained by applying tSNE or UMAP to the output of the embedding layer. The second fully connected layer has dimension equal to the number of cell types in scRNA-seq data. Through a softmax transformation, this layer outputs a probability vector for cell type prediction. For cells in scRNA-seq, this layer can be trained in a supervised fashion using the cross entropy loss.

Given S scRNA-seq experiments with expression matrices and T scATAC-seq experiments with gene activity score matrices, assume suitable intersections have been taken so that all matrices have the same set of genes. Let $\{x_i^{(s)}\}_{i=1}^{N_s}$ be the expression profiles of cells after preprocessing from a scRNA-seq dataset indexed by $s \in \{1, \dots, S\}$, and $\{y_i^{(s)}\}_{i=1}^{N_s}$ be the corresponding cell type annotations. Here each $x_i^{(s)}$ is a G -dimensional vector, where G is the number of genes; $y_i^{(s)} \in \{1, \dots, K\}$, where K is the number of cell types; N_s is the number of cells in experiment s . Similarly, let $\{x_i^{(t)}\}_{i=1}^{N_t}$ be the vectors of gene activity scores after preprocessing from the t -th scATAC-seq dataset with N_t cells ($t \in \{1, \dots, T\}$), whose cell types are unlabelled. The neural network is parametrised by a set of weights and biases, collectively denoted θ . Let $f_{\theta,i}^{(s)} = f(x_i^{(s)}; \theta) \in \mathbb{R}^D$, $D = 64$, be the output of the embedding layer when the input $x_i^{(s)}$ has gone through a transformation of f parametrised by θ . Similarly $g_{\theta,i}^{(s)} = \text{softmax}(h(f(x_i^{(s)}; \theta)))$, where h denotes the output from the prediction layer that goes through the softmax transformation. Thus $g_{\theta,i}^{(s)}$ is a probability vector after the softmax transformation. $f_{\theta,i}^{(t)}$ and $g_{\theta,i}^{(t)}$ are defined in the same way for input $x_i^{(t)}$ from scATAC-seq.

The training of scJoint consists of three steps.

Step 1: Joint neural network based dimension reduction (NNDR) and semi-supervised transfer learning

We first perform joint dimension reduction and feature alignment by imposing suitable loss functions on the outputs of the two fully connected layers. A mini-batch \mathcal{B}_0 of data for training is constructed by sampling equal-sized subsets of cells from each dataset, that is, $\mathcal{B}_0 = \{\mathcal{B}^{(s)}\}_{s=1}^S \cup \{\mathcal{B}^{(t)}\}_{t=1}^T$, where each subset $\mathcal{B}^{(s)}$ (or $\mathcal{B}^{(t)}$) has B cells.

1. **NNDR Loss.** In a spirit similar to PCA, the NNDR loss aims to capture low dimensional, orthogonal features when projecting each data batch into the embedding space. For now we omit the dataset-specific superscript with the understanding that this loss function is applied to each $\mathcal{B}^{(s)}$ and $\mathcal{B}^{(t)}$. Given input vectors $\{x_b\}_{b \in \mathcal{B}}$, define

$\bar{f}_{\theta,\cdot} = \frac{1}{B} \sum_{b \in \mathcal{B}} f_{\theta,b} \in \mathbb{R}^D$, and $\Sigma_{\theta,\cdot}$ as the sample correlation matrix. The NNDR loss is:

$$\mathcal{L}_{\text{NNDR}}(\mathcal{B}, \theta) = \left(\frac{1}{BD} \sum_{b \in \mathcal{B}} \sum_{j=1}^D |f_{\theta,b}(j) - \bar{f}_{\theta,\cdot}(j)| \right)^{-1} + \frac{1}{D^2} \sum_{i \neq j} |\Sigma_{\theta,\cdot}(i, j)| + \frac{1}{BD} \sum_{b \in \mathcal{B}} \sum_{j=1}^D |\bar{f}_{\theta,\cdot}(j)|.$$

Note that to minimise this loss, we maximise the variability within each coordinate (inverse of the first term) and minimise the correlation between all coordinate pairs (the second term) to achieve orthogonality. The last term tries to fix the means of all coordinates near zero for model identifiability, preventing θ from drifting to unstable regions of the parameter space.

2. *Cosine similarity loss.* This loss is applied to the embedding layer outputs from $\mathcal{B}^{(t)}$ and $\mathcal{B}_R = \cup_{s=1}^S \{\mathcal{B}^{(s)}\}$, for every t , and attempts to maximise the similarity between best aligned ATAC and RNA data pairs. Let p be the fraction of data pairs we expect to have high cosine similarity scores. Setting $p < 1$ accounts for situations where RNA and ATAC do not share all their cell types. We set $p = 0.8$ for all the results presented in the paper, although our results appear to be stable with respect to this parameter (Supplementary Figure S16a). Recall that for a pair of general vectors (u, v) , the cosine similarity is defined as $\cos(u, v) = \langle u, v \rangle / (\|u\| \|v\|)$. For each $x_b^{(t)}$ with $b \in \mathcal{B}^{(t)}$, we find the corresponding $i(b) \in \mathcal{B}_R$ with input $x_{i(b)}$ that maximises $\cos(f_{\theta,b}^{(t)}, f_{\theta,i(b)})$. From $\mathcal{B}^{(t)}$, we then choose the top p fraction of cells with the highest cosine score and denote the index set \mathcal{I}_p . (\mathcal{I}_p has size $\lfloor Bp \rfloor$.) The loss is given by

$$\mathcal{L}_{\text{cos}}(\mathcal{B}^{(t)}, \mathcal{B}_R, \theta) = -\frac{1}{\lfloor Bp \rfloor} \sum_{b \in \mathcal{I}_p} \cos(f_{\theta,b}^{(t)}, f_{\theta,i(b)}).$$

3. *Cross entropy loss.* For every $\mathcal{B}^{(s)}$ with cell type annotations $\{y_b^{(s)}\}_{b \in \mathcal{B}^{(s)}}$, we apply the cross entropy loss to the prediction layer after softmax transformation to supervise the learning of scRNA-seq datasets:

$$\mathcal{L}_{\text{entropy}}(\mathcal{B}^{(s)}, \theta) = -\frac{1}{B} \sum_{b \in \mathcal{B}^{(s)}} \sum_{k=1}^K 1(y_b^{(s)} = k) \log g_{\theta,b}^{(s)}(k),$$

where $1(\cdot)$ is an indicator function.

In Step 1, the final loss function we minimise with respect to θ for a mini-batch \mathcal{B}_0 is

$$\mathcal{L}_1(\mathcal{B}_0, \theta) = \sum_{s=1}^S (\mathcal{L}_{\text{NNDR}}(\mathcal{B}^{(s)}, \theta) + \mathcal{L}_{\text{entropy}}(\mathcal{B}^{(s)}, \theta)) + \sum_{t=1}^T (\mathcal{L}_{\text{NNDR}}(\mathcal{B}^{(t)}, \theta) + \mathcal{L}_{\text{cos}}(\mathcal{B}^{(t)}, \mathcal{B}_R, \theta)).$$

Step 2: Cell type label transfer by KNN in joint embedding space

The output of Step 1 is a joint embedding space that has roughly aligned RNA and ATAC with cells from either modality lying close if they have similar low dimensional representations in this space. Therefore using the embedding vectors for cells in all the datasets and

calculating the Euclidean distances, we can determine the KNN among all RNA cells for each cell i in ATAC; denote this set of RNA cells $\mathcal{N}(i)$. The cell type label of i is estimated via majority vote using $\{y_j\}_{j \in \mathcal{N}(i)}$. All the results in the paper were obtained from using 30 nearest neighbours. Let the majority cell type be k^* , then the probability score of cell type prediction for cell i in ATAC is an average of its nearest neighbours in RNA. Since for each $j \in \mathcal{N}(i)$, $g_{\theta,j}$ is already a probability vector after the softmax transformation, we take $p_{\theta,j} = g_{\theta,j}(k^*)$ as the probability score of RNA cell j in the majority class $\mathcal{M}(i) \subset \mathcal{N}(i)$. For other $j \in \mathcal{N}(i) \setminus \mathcal{M}(i)$, we threshold the probability score as 0. Then the probability score of ATAC cell i is calculated as

$$\hat{p}_{\theta,i} = \frac{1}{30} \sum_{j \in \mathcal{M}(i)} p_{\theta,j}.$$

Step 3: Joint training with transferred cell type labels

In the final step of the training, we refine the joint embedding space and improve mixing of cells from the same cell type using the transferred labels from Step 2. We include an additional loss function commonly used in metric learning for enhancing embedded clustering structure given labelled data. The other loss functions and network architecture remain the same as Step 1 with ATAC cells and their transferred labels added to $\mathcal{L}_{\text{entropy}}$.

For each cell type $k \in \{1, \dots, K\}$, we initialise the class centre $c_k \in \mathbb{R}^D$ randomly. We construct mini-batches of cells from all the datasets in the same way as Step 1. Now that all cells have cell type labels (given or transferred), for convenience we will refer to cells in a mini-batch \mathcal{B}_0 without explicitly labeling which dataset they come from. For a given \mathcal{B}_0 , we first update the class centres by taking the average of c_k and $\{f_{\theta,b}\}$ with $b \in \mathcal{B}_0$ and $y_b = k$. Let the updated centres be c'_k . As the number of mini-batches grows, the influence of the initial c_k becomes negligible. The metric learning loss we use is the centre loss:

$$\mathcal{L}_{\text{centre}}(\mathcal{B}_0, \theta) = \frac{1}{|\mathcal{B}_0|K} \sum_{b \in \mathcal{B}_0} \sum_{k=1}^K \|f_{\theta,b} - c'_k\|^2 1(y_b = k).$$

The total loss function we minimise in Step 3 is given by

$$\mathcal{L}_{\text{scJoint}}(\mathcal{B}_0, \theta) = \mathcal{L}_1(\mathcal{B}_0, \theta) + \mathcal{L}_{\text{centre}}(\mathcal{B}_0, \theta).$$

We perform a final round of majority vote by KNN using distances in the embedding space. If the prediction of any ATAC cell is different from Step 2, we update both its prediction and probability score in the same way as Step 2.

Training details

The batch size B was set to 256 in all cases. The other training details including learning rate and number of training epochs used in each dataset can be found in Table S1. We started all the training with learning rate set to 0.01, since a large learning rate has the benefit of faster training. However, if the values of the loss functions were observed to have too much fluctuation, we decreased the learning rate to 0.001 for more stable training.

Data preprocessing

- *Mouse atlas data.* The processed gene expression matrix and the cell type annotation of the Tabula Muris mouse data of scRNA-seq were downloaded from <https://tabula-muris.ds.czbiohub.org/>. The quantitative gene activity score matrix and the cell type annotation of Mouse sci-ATAC-seq Atlas were downloaded from <https://atlas.gs.washington.edu/mouse-atac/>. We manually checked the cell type annotations from the original studies and re-annotated the labels such that the naming convention is consistent across the datasets. For example, the cell type “Cardiac muscle cell” in the sci-ATAC-seq dataset was changed to “Cardiomyocytes”. We also combined some of the cellular subtypes in the sci-ATAC-seq data to increase the percentage of overlapping labels between two atlases for evaluation. More specifically, we combined “Regulatory T cell” and “T cell” into “T cell”; “Immature B cell”, “Activated B cell” and “B cell” into “B cell”; “Excitatory neurons” and “Inhibitory neurons” into “Neuron”.
- *SNARE-seq data.* The SNARE-seq data from adult mouse cerebral cortex was downloaded from the National Center for Biotechnology Information (NCBI) Gene Expression Omnibus (GEO) accession number GSE126074 (8), with both raw gene expression and DNA accessibility measurements available for the same cell. The fastq files were downloaded from the Sequence Read Archive (SRA) for SRP183521. We first derived the fragment files from the fastq files using `sinto fragments` (`sinto v0.7.2`), and then generated the gene activity matrix using Signac (`v1.1.0.9000`) (31). The cell type information was obtained from the original study (8). We filtered out the cells that were originally labelled as “Misc” (cells of miscellaneous cluster), resulting in a dataset with 9190 cells for the integrative analysis.
- *Multi-modal data (CITE-seq and ASAP-seq PBMC data).* The ASAP-seq and CITE-seq data were downloaded from GEO accession number GSE156478 (23), which included the fragment files and antibody-derived tags (ADTs) matrices for ASAP-seq, the raw unique molecular identifier (UMI) and ADT matrices for CITE-seq, from both control and stimulated conditions. The gene activity matrices for ASAP-seq were generated by Signac. Most of the thresholds we used for quality control metrics were consistent with those in the original paper (23). The control and stimulated CITE-seq were filtered based on the following criteria: mitochondrial reads greater than 10%; number of expressed genes less than 500; total number of UMI less than 1000; total number of ADTs from the rat isotype control greater 55 and 65 in the control and stimulated conditions respectively; total number of UMI greater than 12,000 and 20,000 for the control and stimulated conditions respectively; total number of ADTs less than 10,000 and 30,000 for control and stimulated conditions respectively. We further filtered out cells that were classified as doublets in original study. For the ASAP-seq data, we filtered out cells with the number ADTs more than 10,000 and number of peaks more than 100,000. Finally, 4502 cells (control) and 5468 cells (stimulated) from ASAP-seq, 4644 cells (control) and 3474 cells (stimulated) from CITE-seq were included in the downstream analysis. We used CiteFuse to integrate the peak matrix or gene expression matrix with their corresponding protein expression and obtain clustering for ASAP-seq and CITE-seq within each condition separately (14). For ASAP-seq, the similarity matrices of the chromatin accessibility are calculated by applying the Pearson correlation to the TF-IDF transformation of the peak matrix. We then followed the

procedure described in (21) to annotate the clusters.

For scJoint, all the gene expression matrices and gene activity score matrices were binarised as 0 or 1, with 1 representing any non-zero original values, as the final input for training. Binarisation scales the two modalities so that their distributions have the same range and reduces the noise level in the data for easier co-training.

Settings used in other methods

For the unpaired data (mouse cell atlases and multi-modal data from CITE-seq and ASAP-seq), we benchmarked the performance of scJoint against three other methods designed for integrating unpaired single-cell multi-modal data: Seurat (v3), Conos and Liger. We compared the label transfer accuracy with Seurat and Conos and the joint visualisations with all three methods. For the paired data (SNARE-seq), we further compared joint visualisations with two methods specifically designed for paired data, scAI and MOFA+. For all the unpaired methods, we used gene activity matrices derived from the above data preprocessing step as input for scATAC-seq. For the two paired methods, we used the peak matrices of scATAC-seq data as input. Detailed settings used in each method are as follows.

- *Seurat*. R package Seurat v3.2.0 (29) was used for all the datasets. The raw count matrix of scRNA-seq and unnormalised gene activity score matrix of scATAC-seq were used as input, which were then normalised using the `NormalizeData` function in Seurat. Noted that for the CITE-seq and ASAP-seq data, the input was a concatenated matrix of log-transformed normalized gene expression data/gene activity score matrix and log-transformed ADTs matrix. Top 2000 most variable genes were selected from scRNA-seq using `FindVariableFeatures` with `vst` as method. To identify the anchors between scRNA-seq and scATAC-seq data, `FindTransferAnchors` function was used with “cca” as reduction method. The scATAC-seq data was then imputed using `TransferAnchors` function, where the anchors were weighted by latent semantic indexing (LSI) reduced dimension of scATAC-seq. Principal component analysis was then performed on the merged matrix of scRNA-seq data and imputed scATAC-seq data. For all the datasets, 30 principal components (PCs) were used for joint visualisation with tSNE (function `RunTSNE`).

For the mouse cell atlas data, we first integrated the two scRNA-seq datasets (FACS and droplet) using `FindIntegrationAnchors` and `IntegrateData`, and then the integrated matrix was scaled using `ScaleData` and used as reference to find transfer anchors.

- *Conos*. R package conos v1.3.1 (5) was used for all the datasets. Function `basicP2proc` in `pagoda2` package (v0.1.2) was performed to process the raw count matrix of scRNA-seq and unnormalised gene activity score matrix of scATAC-seq. The joint graph was built using `buildGraph` with `k=15`, `k.self=5`, and `k.self.weigh=0.01`, which were set as suggested in the tutorial for integrating RNA and ATAC (http://pklab.med.harvard.edu/peterk/conos/atac_rna/example.html). The joint visualisation of scRNA-seq and scATAC-seq were generated using `largeVis` by `embedGraph`, which is the default visualisation in Conos.
- *Liger*. R package liger v0.5.0 (35) was used for the datasets. The raw count matrix of scRNA-seq and unnormalised gene activity score matrix of scATAC-seq were used

as input, which were normalised using `normalize` function in `liger`. Highly variable genes were selected using the scRNA-seq. For the mouse cell atlas data, both FACS and droplet scRNA-seq data were used to select features. For all the datasets, number of factors was set to 20 in `optimizeALS`. tSNE was then performed on the normalized cell factors to generate the joint visualisation of scRNA-seq and scATAC-seq (function `runTSNE` in `liger`).

- *scAI*. R package *scAI* v1.0.0 (13) was used for the integration of SNARE-seq data. The raw count matrix of scRNA-seq and raw peak matrix of scATAC-seq were used as input. We ran *scAI* using `run_scAI` by setting the rank of the inferred factor set as 20, `do.fast = TRUE`, and `nrun = 1`, with other parameters set as default, as suggested in the pipeline in the github repository. tSNE plots were generated using `reducedDims` function in *scAI*.
- *MOFA+*. R package *MOFA2* v1.0 (4) was used for the integration of SNARE-seq data. Following the suggested integration tutorial for SNARE-seq in the github repository, we first selected top 2500 most variable genes using `FindVariableFeatures` in *Seurat* package with `vst` as method and top 5000 most variable ATAC peaks with `disp` as method. By subsetting the counts matrix of scRNA-seq and peak matrix of scATAC-seq with the selected features, we ran *MOFA+* by setting the number of factors as 10, with other parameters set as default. tSNE plots were generated using `run_tsne` function in *MOFA2*.

Evaluation metrics

Joint embedding evaluation - Silhouette coefficients

To evaluate whether the joint embeddings from different methods show clustering structure reflecting biological signals or technical variations, we calculated the silhouette coefficient for each cell by considering two different groupings: (1) grouping based on the modalities (scRNA-seq or scATAC-seq), called the modality silhouette coefficient ($s_{modality}$); (2) grouping based on known cell types, called the cell type silhouette coefficient ($s_{cellTypes}$). Note that for the atlas data, we consider FACS and droplet in scRNA-seq as two distinct technologies and the modality silhouette coefficient has three groups (FACS, droplet, ATAC) in the calculation. For SNARE-seq, the paired methods (*scAI* and *MOFA+*) have no modality silhouette coefficients since each cell has one paired profile of RNA and ATAC. An ideal joint visualisation should have low modality silhouette coefficients, suggesting the removal of the technical effect, and large cell type silhouette coefficients, indicating the cells are grouped by cell types. The euclidean distance for all methods except *Conos* is obtained from the tSNE embedding. For *Conos*, the distance is obtained from the `largeVis` embedding, which is the method's default output.

We then summarise the two silhouette coefficients by calculating an F1-score as follows:

$$F1_{sil} = \frac{2 \cdot (1 - s'_{modality}) \cdot s'_{cellTypes}}{1 - s'_{modality} + s'_{cellTypes}},$$

where $s' = (s + 1)/2$. A higher F1 score indicates better performance in the alignment of the modalities as well as the preservation of biological signals.

Accuracy evaluation of transferred labels

We evaluated the accuracy of label transfer from two aspects: (1) Overall accuracy rate; (2) Cell type classification F1-score. The overall accuracy rate was computed only accounting for the common cell types between scRNA-seq and scATAC-seq data. The cell type classification F1-score is the harmonic mean of precision and recall of each cell type.

Software availability

scJoint was implemented using PyTorch (version 1.0.0) with code available at <https://github.com/SydneyBioX/scJoint>.

Acknowledgments

The authors gratefully acknowledge the following funding sources: Research Training Program Tuition Fee Offset and Stipend Scholarship and Chen Family Research Scholarship to Y.L.; Australian Research Council Discovery Project grant (DP170100654) to J.Y.H.Y.; Australian Research Council DECRA Fellowship (DE180101252) to Y.X.R.W.; NIH grants R01 HG010359 and P50 HG007735 to W.H.W.

Author contributions

T.W., Y.X.R.W. and W.H.W. conceived and designed this project; Y.L., T.W. and S.W. performed data preprocessing, model development, and evaluation of results; J.Y.H.Y., Y.X.R.W. and W.H.W. supervised the execution; Y.L., J.Y.H.Y., Y.X.R.W. and W.H.W. wrote the manuscript. All authors read and approved the manuscript.

Conflict of interest

The authors declare that they have no conflict of interest.

References

- [1] Tamim Abdelaal, Lieke Michielsen, Davy Cats, Dylan Hoogduin, Hailiang Mei, Marcel JT Reinders, and Ahmed Mahfouz. A comparison of automatic cell identification methods for single-cell rna sequencing data. *Genome biology*, 20(1):194, 2019.
- [2] Matthew Amodio and Smita Krishnaswamy. Magan: Aligning biological manifolds. *arXiv preprint arXiv:1803.00385*, 2018.
- [3] Matthew Amodio, David Van Dijk, Krishnan Srinivasan, William S Chen, Hussein Mohsen, Kevin R Moon, Allison Campbell, Yujiao Zhao, Xiaomei Wang, Manjunatha Venkataswamy, et al. Exploring single-cell data with deep multitasking neural networks. *Nature methods*, pages 1–7, 2019.
- [4] Ricard Argelaguet, Damien Arnol, Danila Bredikhin, Yonatan Deloro, Britta Velten, John C Marioni, and Oliver Stegle. Mofa+: a statistical framework for comprehensive integration of multi-modal single-cell data. *Genome Biology*, 21(1):1–17, 2020.
- [5] Nikolas Barkas, Viktor Petukhov, Daria Nikolaeva, Yaroslav Lozinsky, Samuel Demharter, Konstantin Khodosevich, and Peter V Kharchenko. Joint analysis of heterogeneous single-cell rna-seq dataset collections. *Nature methods*, 16(8):695–698, 2019.
- [6] Shelley L Berger. The complex language of chromatin regulation during transcription. *Nature*, 447(7143):407–412, 2007.
- [7] Junyue Cao, Darren A Cusanovich, Vijay Ramani, Delasa Aghamirzaie, Hannah A Pliner, Andrew J Hill, Riza M Daza, Jose L McFaline-Figueroa, Jonathan S Packer, Lena Christiansen, et al. Joint profiling of chromatin accessibility and gene expression in thousands of single cells. *Science*, 361(6409):1380–1385, 2018.
- [8] Song Chen, Blue B Lake, and Kun Zhang. High-throughput sequencing of the transcriptome and chromatin accessibility in the same cell. *Nature biotechnology*, 37(12):1452–1457, 2019.
- [9] Darren A Cusanovich, Andrew J Hill, Delasa Aghamirzaie, Riza M Daza, Hannah A Pliner, Joel B Berletch, Galina N Filippova, Xingfan Huang, Lena Christiansen, William S DeWitt, et al. A single-cell atlas of in vivo mammalian chromatin accessibility. *Cell*, 174(5):1309–1324, 2018.
- [10] Zhana Duren, Xi Chen, Mahdi Zamanighomi, Wanwen Zeng, Ansuman T Satpathy, Howard Y Chang, Yong Wang, and Wing Hung Wong. Integrative analysis of single-cell genomics data by coupled nonnegative matrix factorizations. *Proceedings of the National Academy of Sciences*, 115(30):7723–7728, 2018.
- [11] Greg Finak, Andrew McDavid, Masanao Yajima, Jingyuan Deng, Vivian Gersuk, Alex K Shalek, Chloe K Slichter, Hannah W Miller, M Juliana McElrath, Martin Prlic, et al. Mast: a flexible statistical framework for assessing transcriptional changes and characterizing heterogeneity in single-cell rna sequencing data. *Genome biology*, 16(1):1–13, 2015.

- [12] Dale I Godfrey, H Robson MacDonald, Mitchell Kronenberg, Mark J Smyth, and Luc Van Kaer. Nkt cells: what's in a name? *Nature Reviews Immunology*, 4(3):231–237, 2004.
- [13] Suoqin Jin, Lihua Zhang, and Qing Nie. scai: an unsupervised approach for the integrative analysis of parallel single-cell transcriptomic and epigenomic profiles. *Genome biology*, 21(1):1–19, 2020.
- [14] Hani Jieun Kim, Yingxin Lin, Thomas A Geddes, Jean Yee Hwa Yang, and Pengyi Yang. Citefuse enables multi-modal analysis of cite-seq data. *Bioinformatics*, 36(14):4137–4143, 2020.
- [15] Sandy L Klemm, Zohar Shipony, and William J Greenleaf. Chromatin accessibility and the regulatory epigenome. *Nature Reviews Genetics*, 20(4):207–220, 2019.
- [16] Ilya Korsunsky, Nghia Millard, Jean Fan, Kamil Slowikowski, Fan Zhang, Kevin Wei, Yuriy Baglaenko, Michael Brenner, Po-ru Loh, and Soumya Raychaudhuri. Fast, sensitive and accurate integration of single-cell data with harmony. *Nature methods*, pages 1–8, 2019.
- [17] Yingxin Lin, Shila Ghazanfar, Kevin YX Wang, Johann A Gagnon-Bartsch, Kitty K Lo, Xianbin Su, Ze-Guang Han, John T Ormerod, Terence P Speed, Pengyi Yang, et al. scmerge leverages factor analysis, stable expression, and pseudoreplication to merge multiple single-cell rna-seq datasets. *Proceedings of the National Academy of Sciences*, 116(20):9775–9784, 2019.
- [18] Jie Liu, Yuanhao Huang, Ritambhara Singh, Jean-Philippe Vert, and William Stafford Noble. Jointly embedding multiple single-cell omics measurements. *BioRxiv*, page 644310, 2019.
- [19] Romain Lopez, Jeffrey Regier, Michael B Cole, Michael I Jordan, and Nir Yosef. Deep generative modeling for single-cell transcriptomics. *Nature methods*, 15(12):1053–1058, 2018.
- [20] Laurens van der Maaten and Geoffrey Hinton. Visualizing data using t-sne. *Journal of machine learning research*, 9(Nov):2579–2605, 2008.
- [21] Holden T Maecker, J Philip McCoy, and Robert Nussenblatt. Standardizing immunophenotyping for the human immunology project. *Nature Reviews Immunology*, 12(3):191–200, 2012.
- [22] Leland McInnes, John Healy, and James Melville. Umap: Uniform manifold approximation and projection for dimension reduction. *arXiv preprint arXiv:1802.03426*, 2018.
- [23] Eleni P Mimitou, Caleb A Lareau, Kelvin Y Chen, Andre L Zorzetto-Fernandes, Yusuke Takeshima, Wendy Luo, Tse-Shun Huang, Bertrand Yeung, Pratiksha I Thakore, James Badger Wing, et al. Scalable, multimodal profiling of chromatin accessibility and protein levels in single cells. *bioRxiv*, 2020.
- [24] Hannah A Pliner, Jonathan S Packer, José L McFaline-Figueroa, Darren A Cusanovich, Riza M Daza, Delasa Aghamirzaie, Sanjay Srivatsan, Xiaojie Qiu, Dana Jackson, Anna

- Minkina, et al. Cicero predicts cis-regulatory dna interactions from single-cell chromatin accessibility data. *Molecular cell*, 71(5):858–871, 2018.
- [25] Sebastian Pott and Jason D Lieb. Single-cell atac-seq: strength in numbers. *Genome Biology*, 16(1):172, 2015.
- [26] Aviv Regev, Sarah A Teichmann, Eric S Lander, Ido Amit, Christophe Benoist, Ewan Birney, Bernd Bodenmiller, Peter Campbell, Piero Carninci, Menna Clatworthy, et al. Science forum: the human cell atlas. *Elife*, 6:e27041, 2017.
- [27] Nicholas Schaum, Jim Karkanias, Norma F Neff, Andrew P May, Stephen R Quake, Tony Wyss-Coray, Spyros Darmanis, Joshua Batson, Olga Botvinnik, Michelle B Chen, et al. Single-cell transcriptomics of 20 mouse organs creates a tabula muris: The tabula muris consortium. *Nature*, 562(7727):367, 2018.
- [28] Marlon Stoeckius, Christoph Hafemeister, William Stephenson, Brian Houck-Loomis, Pratip K Chattopadhyay, Harold Swerdlow, Rahul Satija, and Peter Smibert. Simultaneous epitope and transcriptome measurement in single cells. *Nature methods*, 14(9):865, 2017.
- [29] Tim Stuart, Andrew Butler, Paul Hoffman, Christoph Hafemeister, Efthymia Papalexi, William M Mauck III, Yuhan Hao, Marlon Stoeckius, Peter Smibert, and Rahul Satija. Comprehensive integration of single-cell data. *Cell*, 177(7):1888–1902, 2019.
- [30] Tim Stuart and Rahul Satija. Integrative single-cell analysis. *Nature Reviews Genetics*, 20(5):257–272, 2019.
- [31] Tim Stuart, Avi Srivastava, Caleb Lareau, and Rahul Satija. Multimodal single-cell chromatin analysis with signac. *bioRxiv*, 2020.
- [32] Jingshu Wang, Divyansh Agarwal, Mo Huang, Gang Hu, Zilu Zhou, Chengzhong Ye, and Nancy R Zhang. Data denoising with transfer learning in single-cell transcriptomics. *Nature methods*, 16(9):875–878, 2019.
- [33] Tongxin Wang, Travis S Johnson, Wei Shao, Zixiao Lu, Bryan R Helm, Jie Zhang, and Kun Huang. Bermuda: a novel deep transfer learning method for single-cell rna sequencing batch correction reveals hidden high-resolution cellular subtypes. *Genome biology*, 20(1):1–15, 2019.
- [34] Joshua D Welch, Alexander J Hartemink, and Jan F Prins. Matcher: manifold alignment reveals correspondence between single cell transcriptome and epigenome dynamics. *Genome biology*, 18(1):1–19, 2017.
- [35] Joshua D Welch, Velina Kozareva, Ashley Ferreira, Charles Vanderburg, Carly Martin, and Evan Z Macosko. Single-cell multi-omic integration compares and contrasts features of brain cell identity. *Cell*, 177(7):1873–1887, 2019.
- [36] Lei Xiong, Kui Xu, Kang Tian, Yanqiu Shao, Lei Tang, Ge Gao, Michael Zhang, Tao Jiang, and Qiangfeng Cliff Zhang. Scale method for single-cell atac-seq analysis via latent feature extraction. *Nature communications*, 10(1):1–10, 2019.

- [37] Jason Yosinski, Jeff Clune, Anh Nguyen, Thomas Fuchs, and Hod Lipson. Understanding neural networks through deep visualization. *arXiv preprint arXiv:1506.06579*, 2015.